analytical chemistry

Article

pubs.acs.org/ac

Coupling of Phosphate-Imprinted Mesoporous Silica Nanoparticles-Based Selective Enrichment with Matrix-Assisted Laser Desorption Ionization-Time-of-Flight Mass Spectrometry for Highly Efficient Analysis of Protein Phosphorylation

Yang Chen, Daojin Li, Zijun Bie, Xinpei He, and Zhen Liu*

State Key Laboratory of Analytical Chemistry for Life Science, School of Chemistry and Chemical Engineering, Nanjing University, Nanjing 210023, China

Supporting Information

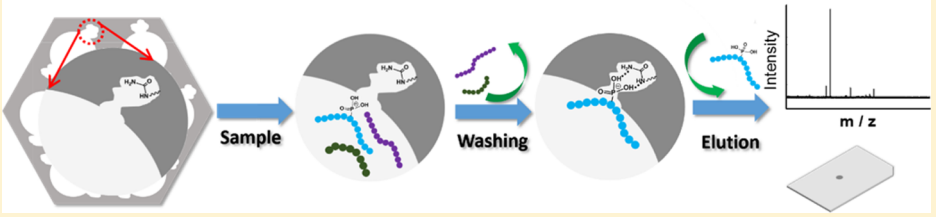

ABSTRACT: Protein phosphorylation is a major post-translational modification and represents a ubiquitous mechanism for the cellular signaling of many different biological processes. Selective enrichment of phosphopeptides from the complex biological samples is a key step for the mass spectrometric (MS) analysis of protein phosphorylation. Herein, we present phosphate-imprinted mesoporous silica nanoparticles (MSNs) as an ideal sorbent for selective enrichment of phosphopeptides and an off-line combination with matrix-asisted laser desorption ionization-time-of-flight mass spectrometry (MALDI-TOF MS) for highly efficient analysis of protein phosphorylation. The phosphate-imprinted MSNs were prepared according to a newly reported strategy called dual-template docking oriented molecular imprinting (DTD-OMI). The prepared molecularly imprinted mesoporous material exhibited several significant merits, such as excellent selectivity toward phosphopeptides, tolerance to interference, fast binding equilibrium, and large binding capacity, which made the molecularly imprinted mesoporous material an ideal sorbent for selective enrichment of phosphopeptides. Using β-casein as a representative phosphoprotein, highly efficient phosphorylation analysis by the off-line platform was verified. Phosphorylation analysis of a nonfat milk sample was also well demonstrated. Because of their highly desirable properties, the phosphate-imprinted MSNs could find more applications in the analysis of protein phosphorylation.

Protein phosphorylation, as one of the most important post-translational modification (PTM) in mammalian species, plays a vital role in cellular signaling of numerous biological processes.[1−3] In total, 30% of proteins in the human genome can be phosphorylated and abnormal phosphorylation is recognized as a cause of human disease.[4,5] Since phosphorylation of any site on a certain protein can change the function or localization of the protein, understanding the "state" of a cell requires the detailed analysis of the phosphorylated proteins being involved. Mass spectrometry (MS) has been an indispensable tool for phosphorylation analysis. However, the mass spectrometric analysis of protein phosphorylation is still far from being routine, because it often suffers from low abundance of phosphopeptides, poor ionization efficiency, and signal suppression by abundant nonphosphopeptides. To solve these issues, enrichment of phosphopeptides is essential prior to MS analysis.

To date, a large variety of phospho-specific enrichment techniques have been developed for this purpose, including immunoaffinity,[6,7] chemical coupling,[8] metal oxide affinity chromatography (MOAC),[9−13] strong ion exchange chromatography,[14−16] and immobilized metal ion affinity chromatography (IMAC),[17−25] among which the last one was the most commonly used. However, the bound metal ions were easily lost during the experimental procedure. To overcome this major drawback, Zou and co-workers coupled phosphonate groups for chelation and immobilization of Ti^{4+} via coordination between Ti^{4+} and the P−O bond.[21−23] Such immobilization creates a beneficial structural orientation for the selective binding of phosphopeptides. However, the lack of site selectivity for phosphorylation is still the most challenging obstacles for these chemoaffinity protocols. On the other hand, although antibodies with high selectivity are widely used for profiling phosphorylation species,[26−29] they are hard to prepare, susceptible to denaturation, and most of all, they often fail to recognize certain phosphorylated species due to the

Received: November 16, 2015
Accepted: December 18, 2015
Published: December 18, 2015

DOI: 10.1021/acs.analchem.5b04343
Anal. Chem. 2016, 88, 1447−1454

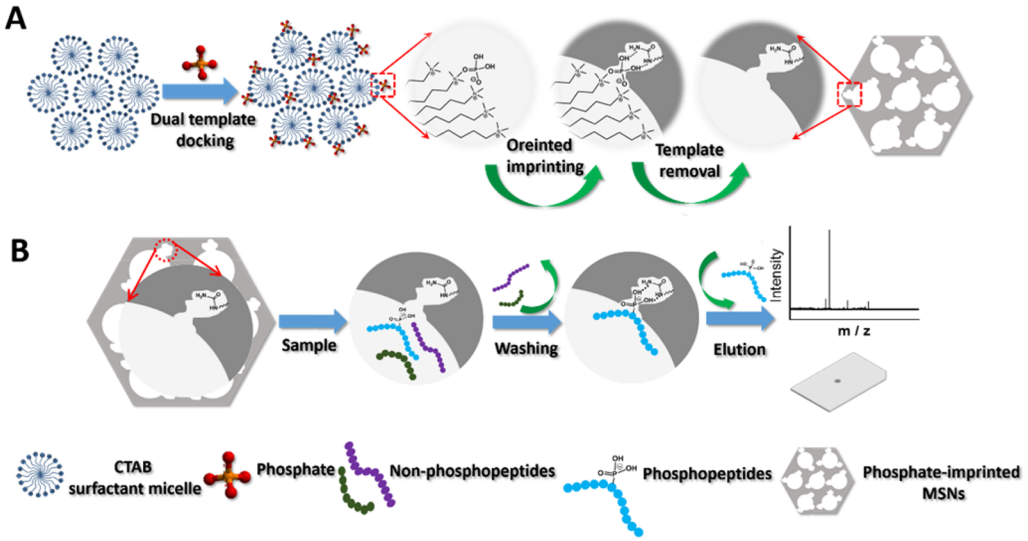

Figure 1. Schematic of (A) the synthesis procedure of phosphate-imprinted MSNs and (B) the procedure of the phosphate-imprinted MSNs-based enrichment-MALDI TOF MS analysis.

stereohindrance effect between antibodies and targets. Therefore, the design and synthesis of novel phospho-specific materials to improve the enrichment efficiency is still important and necessary.

Molecularly imprinted polymers (MIPs),[30−33] as synthetic mimics of antibodies or enzymes, have found important applications such as separation,[34−36] sensing,[37−39] disease diagnosis,[40−42] catalysis,[43,44] and bioimaging.[45−47] In recent years, Sellergren and co-workers have demonstrated the potentials of MIPs in screening specific phosphorylation sites.[48−50] However, the reported MIPs were prepared by a bulk imprinting approach and needed to be crushed and sieved prior to use, which is not only laborious but also suffers from low capacity to slow binding equilibrium. Thus, new material types that can fully demonstrate the usefulness and powerfulness of MIPs are highly desirable. Mesoporous materials possess a regularly ordered pore arrangement, high surface area, and uniform pore size distribution.[51−53] These prominent features of mesoporous materials were well believed to lead to considerable advantages in separation and sample pretreatment.[54−56] Although, both MIPs[32,57] and mesoporous materials[55,58,59] have separately shown promising features in proteomics research. The benefits of mesoporous structure based MIPs in proteomics study have never been explored. Recently, we developed a universal and efficient strategy called dual-template docking oriented molecular imprinting (DTD-OMI) to prepare molecularly imprinted mesoporous materials for small charged molecules.[60] The prepared imprinted mesoporous material shows great potential in real-world applications. This inspired us to further extend the applicable range of this novel material.

In this work, by using this versatile and facile imprinting strategy to engineer phosphate group receptors, we have now developed phosphate-imprinted mesoporous silica nanoparticles (MSNs) and established a hyphenated approach of MIP-based selective enrichment with matrix-assisted laser desorption ionization-time-of-flight (MALDI-TOF) MS for highly efficient phosphorylation analysis. The synthetic procedure of the phosphate-imprinted MSNs was slightly modified from the original version of the DTD-OMI strategy.[60] As illustrated in Figure 1A, the procedure included three main steps: (1) formation of dual-template complexes, in which phosphate (imprinting template) was docked onto the rod-like CTAB micelles (mesopore template) through electrostatic attraction; (2) oriented imprinting, in which an appropriate Si source precursor, specifically a mixture containing tetraethoxysilane (TEOS), 3-ureidopropyltriethoxysilane (UPTES), was introduced to form mesoporous silica nanoparticles; and (3) template removal, in which both the mesoporous template and imprinting template were removed. The obtained mesoporous MIP inherited all favorable features of molecularly imprinted MSNs produced by the DTD-OMI approach. Because of the existence of dual-template docking configuration, all the imprints were imprinted on the wall of the mesopores, and this unique arrangement could provide highly accessible binding sites to phosphopeptides. Meanwhile, owing to the high specific surface area, the imprinted MSNs could provide high binding capacity. Moreover, because of the biocompatible nature of silica, the imprinted MSNs could avoid nonspecific adsorption and interference from abundant non-phosphopeptides. In a word, phosphate-imprinted mesoporous silica nanoparticles could be an ideal sorbent for the selective enrichment of phosphopeptides. By coupling this imprinted material with matrix-assisted laser desorption/ionization time-of-flight mass spectrometry (MALDI-TOF MS), an off-line combined platform was established for efficient phosphorylation analysis. The procedure of the off-line approach is illustrated in Figure 1B, which included four steps: sample loading, washing, eluting, and MS analysis. The phosphate-imprinted MSNs exhibited excellent selectivity, superb tolerance to interference, fast binding equilibrium, and large binding capacity. By using different biological samples, high efficient phosphorylation analysis by this platform was demonstrated.

EXPERIMENTAL SECTION

Reagents and Materials. 3-Ureidopropyltriethoxysilane (UPTES), tetraethoxysilane (TEOS), adenosine monophosphate (AMP), trifluoroacetic acid (TFA), acetonitrile (ACN) of LC−MS grade, trypsin and 2,5-dihydroxybenzoic acid (DHB), bovine β-casein and trypsin were obtained from Sigma (St. Louis, MO). *N*-Cetyltrimethylammonium bromide (CTAB),

DOI: 10.1021/acs.analchem.5b04343
Anal. Chem. 2016, 88, 1447−1454

Na_3PO_4, and all other chemical reagents were of analytical grade and obtained from Sinopharm Chemical Reagent (Shanghai, China). Water used in all the experiments was purified by a Milli-Q Advantage A10 ultrapure water purification system (Millipore, Milford, MA).

Instruments. Transmission electron microscopy (TEM) characterization was performed on a JEM-2100 system (JEOL, Tokyo, Japan). The X-ray diffraction (XRD) patterns of samples were acquired on an ARL XTRA diffractometer (Thermo Fisher Scientific, Waltham, MA) with Cu Kα radiation in the 2θ range of 0.5−6°. The UV absorbance measurement was performed on a NanoDrop 2000/2000C spectrophotometer (Thermo Fisher Scientific, Waltham, MA), and the wavelength was adopted at 260 nm for all the analytes. Nitrogen adsorption−desorption measurements were conducted at 77 K on an ASAP2020 instrument (Micromeritics, Norcross, GA). The surface areas were calculated by the Brunauer−Emmett−Teller (BET) method, and the pore size distributions were calculated by the Barrett−Joyner−Halenda (BJH) method. MALDI-TOF MS analyses were carried out on a 4800 plus MALDI TOF/TOF analyzer (Applied Biosystems, Framingham, MA) with a pulsed nitrogen laser operated at 337 nm. The laser energy was adjusted to slightly above the threshold to obtain good resolution and signal-to-noise ratio (S/N). All mass spectra reported were obtained in the positive ion mode. The instrument was operated in reflectron mode for peptide detection. A typical spectrum was obtained by averaging 3000 laser shots from 30 positions within the sample well. The accelerating voltage was 20 kV. The whole process was controlled by the 4000 series Explorer Software V3.7.0. Data were processed using Data Explorer Software version 3.7 (Applied Biosystems, Framingham, MA). The matrixes for MALDI-TOF MS were 20 mg/mL DHB dissolved in 50% ACN containing 1% (v/v) H_3PO_4. The lyophilized powder of analytes were first dissolved in 2 μL of matrix solution and dropped onto the MALDI plate for MALDI-TOF MS analysis.

Synthesis of Phosphate-Imprinted Mesoporous Silica Nanoparticles. The synthesis of phosphate-imprinted mesoporous silica was modified based on the DTD-OMI strategy.[60] Briefly, 0.3 g of CTAB, 84 mg of NaOH, 144 mL of H_2O were added into a 500 mL round-bottom flask. After the mixture was heated to 80 °C, 76 mg (0.2 mmol) of Na_3PO_4 was added and then stirred for 15 min. Then a mixture of TEOS (4.8 mmol), UPTES (0.2 mmol), and ethanol (100 μL) was added dropwise to the solution under vigorous stirring, and the resulting mixture was allowed to react for 2 h to produce a white precipitate. The solid crude product was filtered and dried under high vacuum to yield the as-synthesized material. To prepare nonimprinted MSNs for comparison, the synthetic procedure was the same except that no template (Na_3PO_4) was added.

Template Removal. To remove the surfactant template and imprinting template in the as-synthesized material, the Soxhlet extraction method was employed. Briefly, a methanolic acidic solution prepared by mixing 1.50 mL of HCl (37.2%) with 150 mL of methanol was used as the extraction solvent. After extraction for 24 h, the material was placed under high vacuum with heating at 60 °C to remove residual solvent within the mesopores to get molecularly imprinted MSNs.

Binding Capacity. Considering the template molecule (Na_3PO_4) has no UV absorbance, AMP was chosen as the test compound for this investigation. Because the AMP molecule contains both phosphate and UV chromophoric group, the employment of AMP will greatly simplify the experimental procedures. For details, 900 μL of 5 mg/mL AMP dissolved in loading buffer (ACN−TFA−H_2O, 70:5:25, v/v/v) was added with 2 mg of molecularly imprinted MSNs. The tube was shaken on a rotator for 20 min at room temperature. The imprinted MSNs were then collected by centrifugation and then washed three times with 200 μL of washing buffer 1 (ACN−TFA−H_2O, 70:5:25, v/v/v) and washing buffer 2 (ACN−TFA−H_2O, 50:1:49, v/v/v). After washing, the imprinted MSNs were resuspended and eluted in 200 μL of 0.4 M NH_4OH by powerful shaking for 10 min on a rotator. Then the imprinted materials were centrifuged again and the eluates were collected by pipetting carefully. Finally, the eluted test compound was vacuum freeze-dried and redissolved in 20 μL of H_2O before UV absorbance measurement. The binding capacity was calculated through the corresponding calibration curve. The measurement was repeated for five parallel experiments, and the averaged value was used as the final binding capacity.

Imprinting Efficiency. Imprinting efficiency, which is defined as the ratio of the number of imprinted cavities of the molecularly imprinted MSNs over the total number of template molecules used in the synthetic procedure, was calculated using related parameters.

Binding Constant. Equivalent molecularly imprinted mesoporous silica (2 mg) was added to solutions (900 μL) of AMP at different concentrations in 1.5 mL plastic microcentrifugal tubes. In order to accurately measure dissociation constants (K_d), the tubes were shaken on a rotator for 2 h (long enough to reach the equilibrium) at room temperature. The washing and elution procedures were the same as those described above. The amounts of AMP extracted by the molecularly imprinted MSNs were determined by measuring the AMP in the eluates through measuring the UV absorbance. Three parallel measurements were carried out for each experimental point. The amount of AMP bound to molecularly imprinted MSNs was plotted according to the Scatchard equation to estimate the binding properties of the material.

Binding Equilibrium. One mg/mL AMP dissolved in dissolved in loading buffer (ACN−TFA−H_2O, 70:5:25, v/v/v) was employed as the sample. A volume of 1 mL of sample solution was added to 2 mg of molecularly imprinted MSNs. After incubation for different time, the washing and elution procedures were the same as those described above. The eluted test compound was vacuum freeze-dried and redissolved in 20 μL of H_2O before UV absorbance measurement.

Tryptic Digestion of Standard Protein. The procedure for the tryptic digest of proteins used in the experiment was prepared as follows: 1 mg of protein was added to a centrifugal vial and dissolved in 1 mL of 100 mM NH_4HCO_3 buffer solution (pH 8.5). After being heated in a water bath of 95 °C for 10 min, the vial was cooled to room temperature. Then the protein solution was digested with trypsin for 18 h at 37 °C (50:1, w/w). Finally, the resulting mixture was heated again to 95 °C and kept for 10 min. The prepared protein digest solution was store at −20 °C.

Selective Enrichment of Phosphopeptides. To prove the selectivity of phosphate-imprinted mesoporous silica prepared by DTD-OMI, the tryptic digestion of β-casein and a mixture of tryptic digestion of β-casein and BSA (w/w, 1:100) were used, respectively. A typical experimental procedure is illustrated in Figure 1B. Briefly, a certain amount of prepared

DOI: 10.1021/acs.analchem.5b04343
Anal. Chem. 2016, 88, 1447−1454

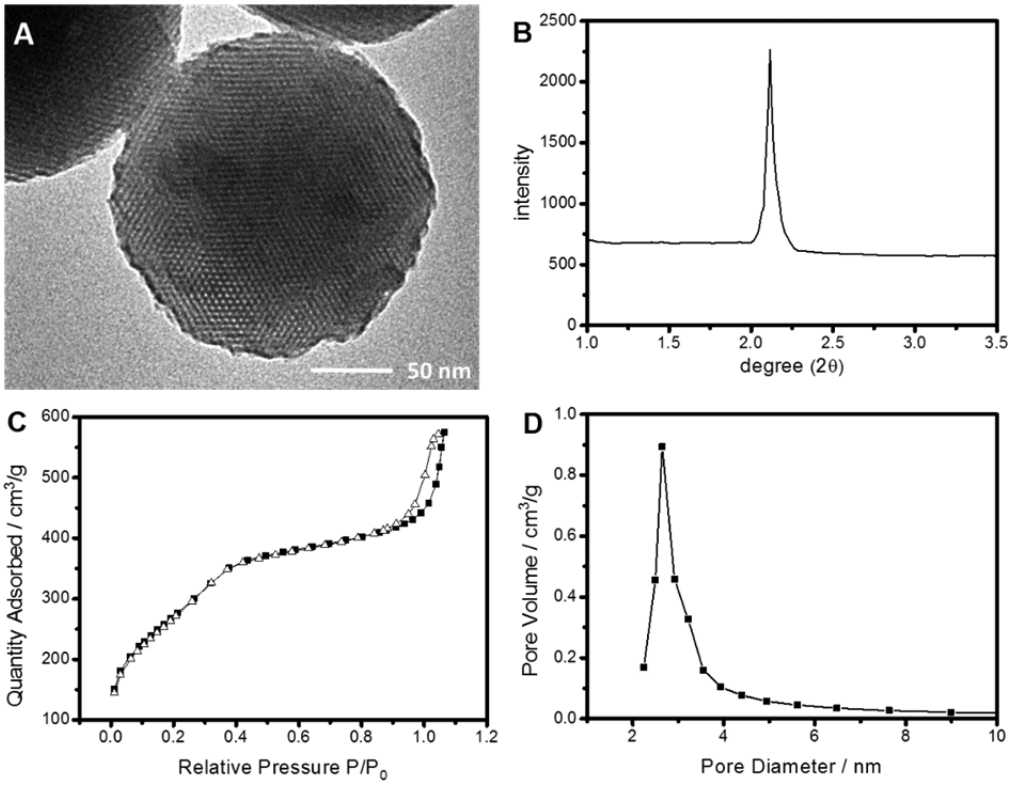

Figure 2. (A) TEM image, (B) XRD pattern, (C) N_2 adsorption−desorption isotherms, and (D) pore size distribution of the phosphate-imprinted MSNs.

imprinting material was first ultrasonically dispread into the loading buffer (ACN−TFA−H_2O, 70:5:25, v/v/v, 500 μg/mL), then 10 μL peptide solution was added to 100 μL of the above-mentioned solution. The tubes were shaken on a rotator for 20 min at room temperature. The washing and elution procedures were the same as those described above. Finally, the eluted phosphopeptides were vacuum freeze-dried and redissolved in 2 μL of matrix solution before MALDI-TOF MS analysis.

Tryptic Digestion of Proteins from Nonfat Milk. A volume of 30 mL of nonfat milk (Mengniu, China) was added into NH_4HCO_3 (1 mL, 25 mM), and this solution was centrifuged at 14 000 rpm for 15 min. The supernatant was collected and then denatured at 100 °C for 10 min. The supernatant was digested with trypsin (40 mg) at 37 °C for 16 h. The prepared digest solution was stored at −20 °C.

Selective Extraction of Digested Phosphopeptides from Nonfat Milk. Briefly, a certain amount of prepared imprinted MSNs was first ultrasonically dispread into the loading buffer (ACN−TFA−H_2O, 70:5:25, v/v/v, 500 μg/mL), then 10 μL of digestion was added to 100 μL of the above-mentioned solution. The tubes were shaken on a rotator for 20 min at room temperature. The washing and elution procedures were the same as those described above. The eluted phosphopeptides was vacuum freeze-dried and redissolved in 2 μL of matrix solution prior to MALDI-TOF MS analysis.

RESULTS AND DISCUSSION

Characterization of the Phosphate-Imprinted MSNs. Figure 2 shows the transmission electron microscopic (TEM) image, X-ray diffraction (XRD) pattern, N_2 adsorption−desorption isotherms, and pore size distribution of the phosphate-imprinted MSNs. The particle size was about 190 nm estimated from the TEM image. The TEM image and the XRD pattern indicate that the imprinted silica nanoparticles possessed excellent mesoporous structure. The mesopore diameter was measured to be 2.6 nm by the Barrett−Joyner−Halenda (BJH) method while the specific surface area was measured to be 792 m^2/g by the Brunauer−Emmett−Teller (BET) method, which obeyed the typical features of mesoporous materials. The high specific surface area is an essential basis for a high binding capacity. The Fourier transform infrared spectroscopy (FT-IR) spectra also provide a solid evidence for the presence of amino and carbonyl groups on the material (Supporting Information, Figure S1).

Choice of Functional Monomer. Functional monomer is one of the most important aspects for molecular imprinting. An appropriate choice of functional monomer will not only ensure the designed binding properties of the material but also greatly simplify the experimental procedure. Although metal ions such as Ti^{4+} and Zr^{4+} were well studied chelating groups for enrichment of phospho-containing molecules,[17−25] the synthesis of this type of materials often needs a multistep procedure. Ureas have long been exploited as neutral hosts for complexing oxyanion guests.[61,62] They can act as two-fold donors and thus can form cyclic hydrogen bonds with hydrogen bond acceptors, such as carboxylate, phosphate, and sulfonate ions. Recently, urea-based phosphate receptors have been reported by Sellergren et al.,[48,49] which showed several apparent advantages, including ease to prepare and ease to operate. Thus, the choice of UPTES will effectively prevent laborious experimental procedure. Besides, the loading and elution conditions for the enrichment of phosphopeptides by urea-based phosphate receptors have also been well studied by Sellergren et al.[50] ACN and TFA of appropriate concentration were added to the loading buffer to increase the affinity

DOI: 10.1021/acs.analchem.5b04343
Anal. Chem. 2016, 88, 1447−1454

between urea group and phosphopeptides while 0.4 M NH_4OH was added to the eluting solution to disrupt the cyclic hydrogen bonds between urea group and phosphopeptides. In this study, we followed similar protocol but slightly changed the concentrations of ACN and TFA.

Optimization of the Imprinting Conditions. The concentration of functional monomer plays an equally important role in the imprinting procedure. If the concentration is too low, the capacity of the material will not be ideally enough. If the concentration is too high, the residual functional groups may lead to the unwanted nonspecific binding sites. Considering this, molar ratio of UPTES to TEOS was optimized and evaluated in terms of imprinting factor (IF). As shown in Figure 3, the obtained MIP exhibited gradually reduced AMP adsorption within the UPTES/TEOS molar ratio range from 1:9 to 0.2:9.8, while the NIPs showed a dramatic drop in AMP adsorption when the ratio range from 1:9 to 0.4:9.6. The best UPTES/TEOS ratio was found to be 0.4:9.6, which gave the highest IF value (5.2).

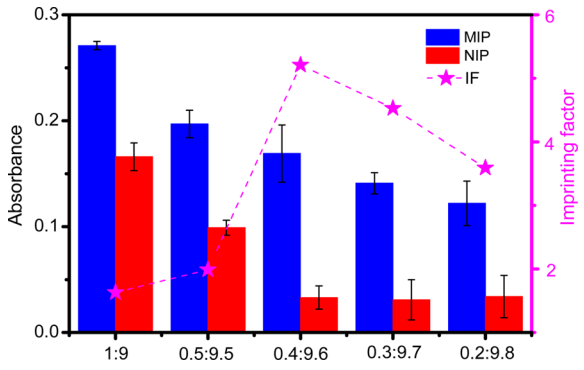

Figure 3. Effects of imprinting condition on the target amount captured by the phosphate-imprinted MSNs and nonimprinted MSNs and on the imprinting factor.

Binding Equilibrium. Binding dynamics of MIPs is an important factor for the feasibility for practical applications. Mesoporous silica, with its most prominent feature of narrow pore size distribution, is well believed to lead to considerable advantages in mass diffusion and transportation of adsorption processes, which lead to fast binding equilibrium. As shown in Figure S2 in the Supporting Information, the binding equilibrium took only 20 min, which is much faster than those required by the monodisperse microsphere (1 h)[21] and the organic MIP (at least 4 h).[48]

Binding Isotherm and Imprinting Efficiency. Figure 4 shows the binding isotherm for phosphate-imprinted MSNs as well as the Scatchard plot for determination of the binding strength according to the Scatchard equation:

$$Q_e/[S] = (Q_{max} - Q_e)/K_d \quad (1)$$

where Q_e is amount of targets bound to molecularly imprinted material at equilibrium, [S] is the free concentration of targets at equilibrium, Q_{max} is the maximum specific binding capacity, and K_d is the dissociation constant. The measured K_d was 71.7 ± 9.1 μM (R^2 = 0.9), which is comparable to the value of previously reported MIP prepared by the DTD-OMI strategy.[49] The maximum specific binding capacity estimated by the Scatchard plot was 359 ± 23 μmol/g. Such a high binding capacity benefited from the high specific surface area of the mesoporous silica nanoparticles on one hand. On the other hand, it benefited from the high imprinting efficiency of the imprinting approach used, which was estimated to be 80% by comparing the maximum amount of phosphate group (AMP) captured by the MIP over that used for the imprinting (450 μmol/g). Such a high imprinting efficiency indicates that a major portion of template molecules eventually produced well-formed binding cavities, which is a unique advantage of the DTD-OMI strategy. Clearly, for templates that are rare or expensive, this high-efficiency imprinting approach is of significant importance.

Method Validation. To demonstrate the selectivity of the phosphate-imprinted MSNs, tryptic digest of a standard phosphoprotein (bovine β-casein) was used to evaluate the performance. The tryptic digest of β-casein was incubated with the phosphate-imprinted MSNs in loading buffer; after isolating the MIP from the solution and washing with washing buffer, the captured phosphopeptides were eluted and deposited on the MALDI target for MALDI-TOF MS analysis. The phosphopeptdes were identified according the theoretical molecular mass values for the fragments from the tryptic digest. As shown in Figure 5A, for the direct analysis of β-casein tryptic digest, only one phosphopeptide with poor signal-to-noise (S/N) ratio was detected due to the relatively low concentration of phosphopeptides and severe signal suppression by the abundant nonphosphopeptides. However, after enrichment by the MIP, three expected phosphopeptides (β1, β2, and β3) were detected with strong MS signal intensities and excellent S/N ratios, along with their four dephosphorylated peptides

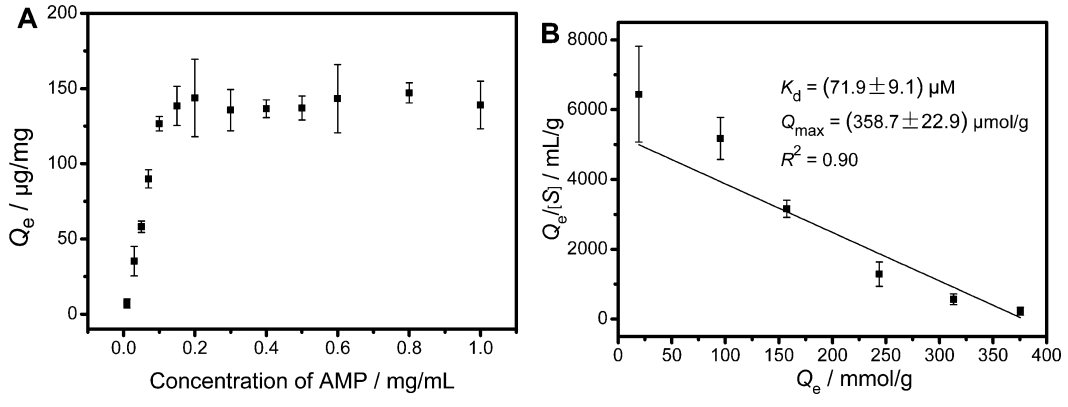

Figure 4. Binding isotherms and corresponding Scatchard plots for phosphate-imprinted MSNs.

DOI: 10.1021/acs.analchem.5b04343
Anal. Chem. 2016, 88, 1447−1454

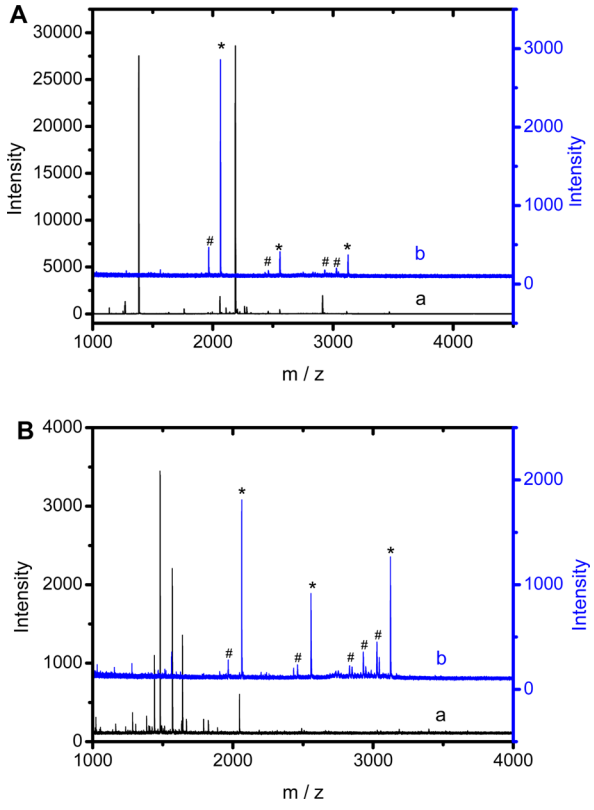

Figure 5. (A) MALDI-TOF mass spectra of the tryptic digest of β-casein. (a) Direct analysis and (b) after enrichment by phosphate-imprinted mesoporous silica. (B) MALDI-TOF mass spectra of the tryptic digest mixture of β-casein and BSA (1:100, w/w). (a) Direct analysis of the peptide mixture and (b) after enrichment by phosphate-imprinted mesoporous silica. The + indicates phosphopeptides and # indicates dephosphorylated peptides.

(Figure 5A), which were likely formed during the MALDI ionization process. The detailed information on the captured phosphopeptides from β-casein is displayed in Table S1 (Supporting Information). For comparison, the tryptic digest of β-casein was treated with nonimprinted MSNs (NIP), and no peaks representing the phosphopeptides were observed (Supporting Information, Figure S3). These results well demonstrated the enrichment selectivity of the phosphate-imprinted mesoporous silica nanoparticles for phosphopeptides. Our previous works proved that rationally synthesized molecularly imprinted materials were able to tolerate severe interference.[32,35,36,42] To further examine such a highly attractive feature for phosphate-imprinted MSNs, a mixture of the tryptic digests of β-casein and BSA was used as the test sample. As shown in Figure 5B, even in the presence of interfering species (nonphosphopeptides from tryptic digest of BSA) at 100-fold higher concentration, the MIP still remained its excellent selectivity for phosphopeptides. For direct analysis of the mixture, no phosphopeptides were detected, while nonphosphopeptide peaks with high MS intensities were observed. However, after extraction by the MIP, three phosphopeptides and their five dephosphorylated peptides were distinctly identified with a clean background. These results confirmed the ability of the MIP for the capture of phosphopeptides from a complex sample.

Practical Application to a Real Sample. To further demonstrate the applicability of the phosphate-imprinted mesoporous silica nanoparticles for selective enrichment of low-abundance phosphopeptides from real samples, nonfat milk was employed as a test sample. As shown in Figure 6, only three

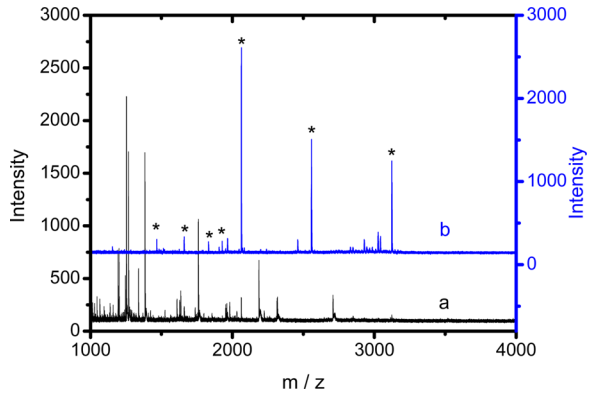

Figure 6. MALDI-TOF mass spectra of tryptic digests of the nonfat milk (a) before and (b) after enrichment by phosphate-imprinted mesoporous silica. The + indicates phosphopeptides.

peaks with low intensities for phosphopeptides were detected with the digested nonfat milk sample and were directly analyzed, which is due to the interference of the abundant nonphosphopeptides; as a comparison, seven peaks of phosphopeptides were distinctly observed after enrichment with the MIP.[63,64] The detailed information on the seven phosphopeptides from the tryptic digest of proteins extracted from nonfat milk is listed in Table S2 (Supporting Information). The results suggested that the phosphate-imprinted mesoporous silica is capable of highly selective enrichment of phosphopeptides from a complex real sample.

CONCLUSION

In this study, we have prepared phosphate-imprinted mesoporous silica nanoparticles for selective enrichment of phosphopeptides and established an off-line combination of MIP-based enrichment with MALDI-TOF MS for highly efficiency phosphorylation analysis. We experimentally demonstrated that the phosphate-imprinted mesoporous silica nanoparticles can be an ideal affinity sorbent for the selective enrichment of phosphopeptides, owing to their significant advantages, including excellent selectivity toward phosphopeptides, tolerance to interference of nonphosphopeptides, fast binding equilibrium and large binding capacity. The performance of the off-line analytical platform was validated using β-casein as a representative phosphoprotein. The feasibility of the proposed method for real-world applications has been well demonstrated with the efficient phosphorylation analysis of nonfat milk. We foresee more promising applications of the phosphate-imprinted mesoporous silica nanoparticles and the off-line coupling approach in phosphorylation analysis.

ASSOCIATED CONTENT

Supporting Information

The Supporting Information is available free of charge on the ACS Publications website at DOI: 10.1021/acs.analchem.5b04343.

Supplementary figures and tables (PDF)

DOI: 10.1021/acs.analchem.5b04343
Anal. Chem. 2016, 88, 1447−1454

AUTHOR INFORMATION

Corresponding Author

*Phone: +86 25 8968 5639. Fax: +86 25 8968 5639. E-mail: zhenliu@nju.edu.cn.

Notes

The authors declare no competing financial interest.

ACKNOWLEDGMENTS

We acknowledge the financial support of the National Science Fund for Distinguished Young Scholars (Grant No. 21425520) and the general grant (Grant No. 21275073) from the National Natural Science Foundation of China as well as the Key Grant of 973 Program (Grant No. 2013CB911202) from the Ministry of Science and Technology of China.

REFERENCES

(1) Hunter, T. *Cell* **2000**, *100*, 113−127.
(2) Ptacek, J.; Devgan, G.; Michaud, G.; Zhu, H.; Zhu, X. W.; Fasolo, J.; Guo, H.; Jona, G.; Breitkreutz, A.; Sopko, R.; McCartney, R. R.; Schmidt, M. C.; Rachidi, N.; Lee, S. J.; Mah, A. S.; Meng, L. H.; Stark, M. J. R.; Stern, D. F.; De Virgilio, C.; Tyers, D. M.; Andrews, B.; Gerstein, M.; Schweitzer, B.; Predki, P. F.; Snyder, M. *Nature* **2005**, *438*, 679−684.
(3) Olsen, J. V.; Blagoev, B.; Gnad, F.; Macek, B.; Kumar, C.; Mortensen, P.; Mann, M. *Cell* **2006**, *127*, 635−648.
(4) Cohen, P. *Nat. Cell Biol.* **2002**, *4*, E127−E130.
(5) Cohen, P. *Trends Biochem. Sci.* **2000**, *25*, 596−601.
(6) Rush, J.; Moritz, A.; Lee, K. A.; Guo, A.; Goss, V. L.; Spek, E. J.; Zhang, H.; Zha, X. M.; Polakiewicz, R. D.; Comb, M. J. *Nat. Biotechnol.* **2005**, *23*, 94−101.
(7) Rikova, K.; Guo, A.; Zeng, Q.; Possemato, A.; Yu, J.; Haack, H.; Nardone, J.; Lee, K.; Reeves, C.; Li, Y.; Hu, Y.; Tan, Z.; Stokes, M.; Sullivan, L.; Mitchell, J.; Wetzel, R.; Macneill, J.; Ren, J. M.; Yuan, J.; Bakalarski, C. E.; Villen, J.; Kornhauser, J. M.; Smith, B.; Li, D.; Zhou, X.; Gygi, S. P.; Gu, T. L.; Polakiewicz, R. D.; Rush, J.; Comb, M. J. *Cell* **2007**, *131*, 1190−1203.
(8) Oda, Y.; Nagasu, T.; Chait, B. T. *Nat. Biotechnol.* **2001**, *19*, 379−382.
(9) Lu, Z. D.; Ye, M. M.; Li, N. W.; Zhong, W. W.; Yin, Y. D. *Angew. Chem., Int. Ed.* **2010**, *49*, 1862−1866.
(10) Pinkse, M. W.; Uitto, P. M.; Hilhorst, M. J.; Ooms, B.; Heck, A. J. *Anal. Chem.* **2004**, *76*, 3935−3943.
(11) Ficarro, S. B.; Parikh, J. R.; Blank, N. C.; Marto, J. A. *Anal. Chem.* **2008**, *80*, 4606−4613.
(12) Min, Q. H.; Zhang, X. X.; Zhang, H. Y.; Zhou, H. F.; Zhu, J. J. *Chem. Commun.* **2011**, *47*, 11709−11711.
(13) Mazanek, M.; Mituloviae, G.; Herzog, F.; Stingl, C.; Hutchins, J. R. A.; Peters, J. M.; Mechtler, K. *Nat. Protoc.* **2007**, *2*, 1059−1061.
(14) Mohammed, S.; Heck, A. J. *Curr. Opin. Biotechnol.* **2011**, *22*, 9−15.
(15) Dong, M. M.; Wu, M. H.; Wang, F. J.; Qin, H. Q.; Han, G. H.; Dong, J.; Wu, R. A.; Ye, M. L.; Liu, Z.; Zou, H. F. *Anal. Chem.* **2010**, *82*, 2907−2915.
(16) Tian, R. J.; Ren, L. B.; Ma, H. J.; Li, X.; Hu, L. H.; Ye, M. L.; Wu, R. A.; Tian, Z. J.; Liu, Z.; Zou, H. F. *J. Chromatogr. A* **2009**, *1216*, 1270−1278.
(17) Nuhse, T. S.; Stensballe, A.; Jensen, O. N.; Peck, S. C. *Mol. Cell. Proteomics* **2003**, *2*, 1234−1243.
(18) Thingholm, T. E.; Jensen, O. N.; Robinson, P. J.; Larsen, M. R. *Mol. Cell. Proteomics* **2007**, *7*, 661−671.
(19) Ye, J. Y.; Zhang, X. M.; Young, C.; Zhao, X. L.; Hao, Q.; Cheng, L.; Jensen, O. N. *J. Proteome Res.* **2010**, *9*, 3561−3573.
(20) Wang, F.; Zhang, Y. T.; Yang, P.; Jin, S.; Yu, M.; Guo, J.; Wang, C. C. *J. Mater. Chem. B* **2014**, *2*, 2575−2582.
(21) Zhou, H. J.; Ye, M. L.; Dong, J.; Corradini, E.; Cristobal, A.; Heck, A. J.; Zou, H. F.; Mohammed, S. *Nat. Protoc.* **2013**, *8*, 461−480.
(22) Feng, S.; Ye, M. L.; Zhou, H. J.; Jiang, X. G.; Jiang, X. N.; Zou, H. F.; Gong, B. L. *Mol. Cell. Proteomics* **2007**, *6*, 1656−1665.
(23) Zhou, H. J.; Ye, M. L.; Dong, J.; Han, G. H.; Jiang, X. N.; Wu, R. A.; Zou, H. F. *J. Proteome Res.* **2008**, *7*, 3957−3967.
(24) Yan, Y. H.; Zheng, Z. F.; Deng, C. H.; Li, Y.; Zhang, X. M.; Yang, P. Y. *Anal. Chem.* **2013**, *85*, 8483−8487.
(25) Xu, X. Q.; Deng, C. H.; Gao, M. X.; Yu, W. J.; Yang, P. Y.; Zhang, X. M. *Adv. Mater.* **2006**, *18*, 3289−3293.
(26) Schindler, C.; Shuai, K.; Prezioso, V. R.; Darnell, J. E. *Science* **1992**, *257*, 809−813.
(27) Seth, A.; Gonzalez, F. A.; Gupta, S.; Raden, D. L.; Davis, R. J. *J. Biol. Chem.* **1992**, *34*, 24796−24804.
(28) Michel, T.; Li, G. K.; Busconi, L. *Proc. Natl. Acad. Sci. U. S. A.* **1993**, *90*, 6252−6256.
(29) Carpenter, C. L.; Auger, K. R.; Duckworth, B. C.; Hou, W. M.; Schaffhausen, B.; Cantley, L. C. *Mol. Cell. Biol.* **1993**, *13*, 1657−1665.
(30) Wulff, G.; Sarhan, A. *Angew. Chem., Int. Ed. Engl.* **1972**, *11*, 341−345.
(31) Vlatakis, G.; Andersson, L. I.; Muller, R.; Mosbach, K. *Nature* **1993**, *361*, 645−647.
(32) Bie, Z. J.; Chen, Y.; Ye, J.; Wang, S. S.; Liu, Z. *Angew. Chem., Int. Ed.* **2015**, *54*, 10211−10215.
(33) Haupt, K.; Mosbach, K. *Chem. Rev.* **2000**, *100*, 2495−2504.
(34) Hart, B. R.; Rush, D. J.; Shea, K. J. *J. Am. Chem. Soc.* **2000**, *122*, 460−465.
(35) Wang, S. S.; Ye, J.; Bie, Z. J.; Liu, Z. *Chem. Sci.* **2014**, *5*, 1135−1140.
(36) Li, L.; Lu, Y.; Bie, Z. J.; Chen, H. Y.; Liu, Z. *Angew. Chem., Int. Ed.* **2013**, *52*, 7451−7454.
(37) Lakshmi, D.; Bossi, A.; Whitcombe, M. J.; Chianella, I.; Fowler, S. A.; Subrahmanyam, S.; Piletska, E. V.; Piletsky, S. A. *Anal. Chem.* **2009**, *81*, 3576−3584.
(38) Bai, W.; Gariano, N. A.; Spivak, D. A. *J. Am. Chem. Soc.* **2013**, *135*, 6977−6984.
(39) Bai, W.; Spivak, D. A. *Angew. Chem., Int. Ed.* **2014**, *53*, 2095−2098.
(40) Bi, X. D.; Liu, Z. *Anal. Chem.* **2014**, *86*, 959−966.
(41) Bi, X. D.; Liu, Z. *Anal. Chem.* **2014**, *86*, 12382−12389.
(42) Ye, J.; Chen, Y.; Liu, Z. *Angew. Chem., Int. Ed.* **2014**, *53*, 10386−10389.
(43) Liu, J. Q.; Wulff, G. *J. Am. Chem. Soc.* **2008**, *130*, 8044−8054.
(44) Ye, L.; Mosbach, K. *Chem. Mater.* **2008**, *20*, 859−868.
(45) Kunath, S.; Panagiotopoulou, M.; Maximilien, J.; Marchyk, N.; Sänger, J.; Haupt, K. *Adv. Healthcare Mater.* **2015**, *4*, 1322−1326.
(46) Shinde, S.; El-Schich, Z.; Malakpour, A.; Wan, W.; Dizeyi, N.; Mohammadi, R.; Rurack, K.; Gjörloff Wingren, A.; Sellergren, B. *J. Am. Chem. Soc.* **2015**, *137*, 13908−13912.
(47) Yin, D. Y.; Wang, S. S.; He, Y. J.; Liu, J.; Zhou, M.; Ouyang, J.; Liu, B. R.; Chen, H. Y.; Liu, Z. *Chem. Commun.* **2015**, *51*, 17696−17699.
(48) Helling, S.; Shinde, S.; Brosseron, F.; Schnabel, A.; Muller, T.; Meyer, H. E.; Marcus, K.; Sellergren, B. *Anal. Chem.* **2011**, *83*, 1862−1865.
(49) Chen, J.; Shinde, S.; Koch, M.; Eisenacher, M.; Galozzi, S.; Lerari, T.; Barkovits, K.; Subedi, P.; Krüger, R.; Kuhlmann, K.; Sellergren, B.; Helling, S.; Marcus, K. *Sci. Rep.* **2015**, *5*, 11438−11449.
(50) Emgenbroich, M.; Borrelli, C.; Shinde, S.; Lazraq, I.; Vilela, F.; Hall, A. J.; Oxelbark, J.; De Lorenzi, E.; Courtois, J.; Simanova, A.; Verhage, J.; Irgum, K.; Karim, K.; Sellergren, B. *Chem. - Eur. J.* **2008**, *14*, 9516−9529.
(51) Tanev, P. T.; Chibwe, M.; Pinnavaia, T. J. *Nature* **1994**, *368*, 321−323.
(52) Corma, A. *Chem. Rev.* **1997**, *97*, 2373−2419.
(53) Wan, Y.; Zhao, D. Y. *Chem. Rev.* **2007**, *107*, 2821−2860.
(54) Xu, Y. W.; Wu, Z. X.; Zhang, L. J.; Lu, H. J.; Yang, P. Y.; Webley, P. A.; Zhao, D. Y. *Anal. Chem.* **2009**, *81*, 503−508.
(55) Qin, H. Q.; Gao, P.; Wang, F. J.; Zhao, L.; Zhu, J. A.; Wang, Q.; Zhang, T.; Wu, R. A.; Zou, H. F. *Angew. Chem., Int. Ed.* **2011**, *50*, 12218−12221.

DOI: 10.1021/acs.analchem.5b04343
Anal. Chem. 2016, 88, 1447−1454

(56) Pan, X. H.; Chen, Y.; Zhao, P. X.; Li, D. J.; Liu, Z. *Angew. Chem., Int. Ed.* **2015**, *54*, 6173−6176.
(57) Jia, X. P.; Xu, M. L.; Wang, Y. Z.; Ran, D.; Yang, S.; Zhang, M. *Analyst* **2013**, *138*, 651−658.
(58) Ma, W. F.; Zhang, Y.; Li, L. L.; You, L. J.; Zhang, P.; Zhang, Y. T.; Li, J. M.; Yu, M.; Guo, J.; Lu, H. J.; Wang, C. C. *ACS Nano* **2012**, *6*, 3179−3188.
(59) Li, Y.; Zhang, X. M.; Deng, C. H. *Chem. Soc. Rev.* **2013**, *42*, 8517−8539.
(60) Chen, Y.; Li, X. L.; Yin, D. Y.; Li, D. J.; Bie, Z. J.; Liu, Z. *Chem. Commun.* **2015**, *51*, 10929−10923.
(61) Fan, E.; Van Arman, S. A.; Kincaid, S.; Hamilton, A. D. *J. Am. Chem. Soc.* **1993**, *115*, 369−370.
(62) Esteban Gomez, D.; Fabbrizzi, L.; Licchelli, M.; Monzani, E. *Org. Biomol. Chem.* **2005**, *3*, 1495−1500.
(63) Xiong, Z. C.; Zhang, L. Y.; Fang, C. L.; Zhang, Q. Q.; Ji, Y. S.; Zhang, Z.; Zhang, W. B.; Zou, H. F. *J. Mater. Chem. B* **2014**, *2*, 4473−4480.
(64) Atakay, M.; Celikbicak, O.; Salih, B. *Anal. Chem.* **2012**, *84*, 2713−2720.

DOI: 10.1021/acs.analchem.5b04343
Anal. Chem. 2016, 88, 1447−1454